Available online at www.sciencedirect.com
ScienceDirect
Journal of Computational Physics 226 (2007) 1985–2002
JOURNAL OF COMPUTATIONAL PHYSICS
www.elsevier.com/locate/jcp

Efficient implementation of THINC scheme: A simple and practical smoothed VOF algorithm ☆

Kensuke Yokoi *

UCLA, Department of Mathematics, Box 951555 Los Angeles, CA 90095-1555, USA
Department of Electronics and Mechanical Engineering, Chiba University, Chiba 263-8522, Japan

Received 26 October 2006; received in revised form 21 June 2007; accepted 23 June 2007
Available online 4 July 2007

Abstract

In this paper, we improve the multi-dimensional THINC (tangent of hyperbola for interface capturing) scheme [F. Xiao, Y. Honma, T. Kono, A simple algebraic interface capturing scheme using hyperbolic tangent function, Int. J. Numer. Meth. Fluid. 48 (2005) 1023]. The THINC scheme is a VOF (volume of fluid) type method. In the original THINC scheme, one-dimensional THINC scheme was straightforwardly used for multi-dimensional cases. In this paper, we propose the WLIC (weighed line interface calculation) method to extend the THINC scheme to multi-dimension. In the WLIC method, the interface is reconstructed by taking an average of line interfaces along x, y and z coordinates with the weights calculated from surface normal. The WLIC method can extend the THINC scheme to multi-dimension while maintaining simplicity of implementation and achieve a higher accuracy than the original THINC scheme. The WLIC method can readily extend the THINC scheme to three-dimension.

Keywords: Interface capturing; Advection scheme; Multi-phase flow; Volume of fluid

1. Introduction

Numerical computations of moving interfaces such as multi-phase flows have many practical and scientific applications. Many numerical methods have been proposed for this kind of numerical simulations, for instance, the front tracking methods [2,3], the level set methods [4–12], the VOF methods [13–36], and the THINC scheme [1]. In the front tracking methods, Lagrangian interfaces are used to track the interface on an Euler grid. The level set methods use the signed distance function to capture the interface. The interface is represented by the zero-level set (zero-contour). The level set methods have advantages for the curvature calculation and are useful to impose boundary conditions at the interface [37–40]. The level set methods have

☆ This work is supported in part by ONR Grant #N00014-03-1-0071 and a Grant-in-Aid for JSPS fellow (17-4063) of Japan Society for the Promotion of Science.
* Tel.: +1 310 206 6958; fax: +1 310 206 6673.
E-mail address: kensuke@math.ucla.edu

0021-9991/$ - see front matter
doi:10.1016/j.jcp.2007.06.020

such advanced features and relatively easy to implement compared to the front tracking method and the VOF methods. Therefore, the level set methods have been used widely. However, the level set methods have a drawback that the level set methods cannot guarantee volume conservation. This causes disappearance of tiny drops.

The VOF methods have been popular in multi-phase flow simulations, because they conserve volume. A type of VOF methods using piecewise linear approximations is highly accurate and has no mass error. However, the methods may not be the most popular methods, because the implementation is difficult. Although the implementation of two-dimensional VOF code is not so difficult, the implementation of three-dimensional VOF code is significantly difficult. Therefore, many people cannot accomplish the implementation, even though they want to use the methods. In this paper, we propose a simple VOF type method. The implementation of the proposed method is as simple as the level set implementation. Although the propose method is not superior to the VOF methods, this method shows similar results with those by the VOF methods.

As an example, now we consider air–liquid two phase flow in two-dimensions. In VOF formulation, the interface is represented by a following characteristic function $\chi(x, y)$:

$$\chi(x,y) = \begin{cases} 1 & \text{for the liquid at the point } (x,y) \\ 0 & \text{for the air at the point } (x,y). \end{cases} \tag{1}$$

Here, I would like to note that $\chi(x, y)$ is the value defined at a point (x, y) and is not a value on a calculation grid. The value on the grid called volume fraction or color function is defined as the cell average of $\chi(x, y)$,

$$C_{i,j} = \frac{1}{\Delta x \Delta y} \int \int_{\Omega_{i,j}} \chi(x,y) \mathrm{d}x \, \mathrm{d}y, \tag{2}$$

where $\Omega_{i,j} = \{(x,y) | x_{i-1/2,j} \leqslant x \leqslant x_{i+1/2,j}, y_{i,j-1/2} \leqslant y \leqslant y_{i,j+1/2}\}$. Although χ has only the value 0 or 1, the volume fraction has the value $0 \leqslant C_{i,j} \leqslant 1$. Fig. 1 is a schematic figure of the characteristic function $\chi(x)$ and the volume fraction C_i in one-dimension.

The characteristic function is developed by the advection equation:

$$\frac{\partial \chi}{\partial t} + \nabla \cdot (\mathbf{u}\chi) - \chi \nabla \cdot \mathbf{u} = 0, \tag{3}$$

where $\mathbf{u}$ is the velocity. $C_{i,j}$ is evolved by an approximation using a dimensional splitting algorithm as follows:

$$C^*_{i,j} = C^n_{i,j} - \frac{F^n_{x,i+1/2,j} - F^n_{x,i-1/2,j}}{\Delta x} + C^n_{i,j} \frac{u_{x,i+1/2,j} - u_{x,i-1/2,j}}{\Delta x} \Delta t, \tag{4}$$

$$C^{n+1}_{i,j} = C^*_{i,j} - \frac{F^*_{y,i,j+1/2} - F^*_{y,i,j-1/2}}{\Delta y} + C^n_{i,j} \frac{u_{y,i,j+1/2} - u_{y,i,j-1/2}}{\Delta y} \Delta t, \tag{5}$$

with

$$F_{x,i+1/2,j} = -\int_{y_{i,j-1/2}}^{y_{i,j+1/2}} \int_{x_{i+1/2,j}}^{x_{x,i+1/2,j} - u_{i+1/2,j}\Delta t} \chi_{is,j}(x,y) \mathrm{d}x \, \mathrm{d}y, \tag{6}$$

$$F_{y,i,j+1/2} = -\int_{y_{i,j+1/2}}^{y_{i,j+1/2} - u_{y,i,j+1/2}\Delta t} \int_{x_{i-1/2,j}}^{x_{i+1/2,j}} \chi_{i,js}(x,y) \mathrm{d}x \, \mathrm{d}y. \tag{7}$$

Here, $F_{x,i+1/2,j}$ and $F_{y,i,j+1/2}$ are the advection fluxes for x direction and y direction, respectively. is and js are

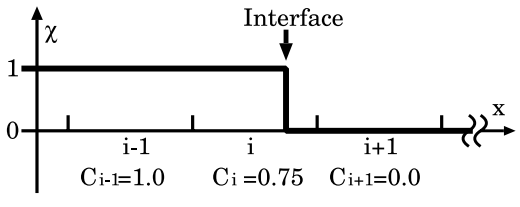

Fig. 1. One-dimensional schematic figure of the characteristic function $\chi(x)$ and the volume fraction C_i.

$$is = \begin{cases} i & \text{if } u_{x,i+1/2,j} \geqslant 0 \\ i+1 & \text{if } u_{x,i+1/2,j} < 0 \end{cases} \tag{8}$$

and

$$js = \begin{cases} j & \text{if } u_{y,i,j+1/2} \geqslant 0 \\ j+1 & \text{if } u_{y,i,j+1/2} < 0, \end{cases} \tag{9}$$

respectively. The order of sweep direction of (4) and (5) is alternated every time step to minimize the error by dimensional splitting.

If $\chi_{i,j}$ is given as shown in Fig 2a, we can easily calculate $C_{i,j}^{n+1}$. However, only the volume fraction $C_{i,j}^{n}$ is given in computation as shown in Fig 2b. The problem in the VOF method is attributed to reconstruction of $\chi_{i,j}$ from the volume fraction $C_{i,j}^{n}$. The VOF methods contain several varieties. Two typical methods to reconstruct $\chi_{i,j}$ are the SLIC (simple line interface calculation) method [13] and the PLIC (piecewise linear interface calculation) method [15]. In the SLIC method (and also the VOF method by Hirt and Nichols [14]), $\chi_{i,j}$ is reconstructed by a line along x or y coordinate as shown in Fig. 3a. An advantage of the SLIC method is easy to implement. In the PLIC method, $\chi_{i,j}$ is calculated based on an diagonal line as shown in Fig. 3b. Although the PLIC method is more accurate than the SLIC method, the implementation is complicated especially for three-dimensional case.

The THINC scheme is almost same with the VOF methods except the characteristic function. Although the VOF methods use the Heaviside step function as the characteristic function, the THINC scheme uses a smoothed Heaviside function as shown in Fig. 4. In the THINC formulation, the surface is represented by the smoothed function. An advantage of the THINC scheme is that it can prevent isolated small fluid (flotsam) as discussed in the section of numerical results. By using a smoothed Heaviside function, the volume fraction $C_{i,j}$ becomes smoother than that of the VOF methods. The feature may be useful for the computation of the normal vector of the interface. Although the THINC scheme can also use reconstruction methods like the

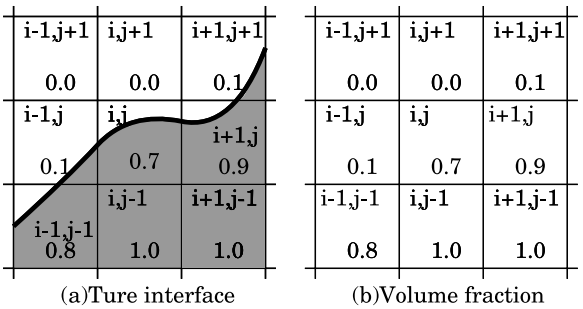

Fig. 2. A schematic figure of two-dimensional volume fraction. The dark part ($\chi(x, y) = 1$) and the white part ($\chi(x,y) = 0$) represent the regions 1 and 0, respectively.

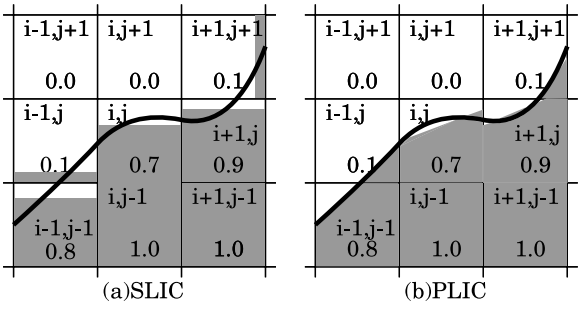

Fig. 3. Interface reconstruction by the SLIC method and the PLIC method.

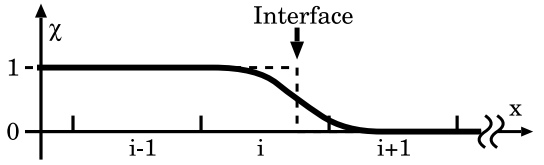

Fig. 4. One-dimensional schematic figure of a THINC characteristic function $\chi(x)$ (bold line). The dot line represents the characteristic function of the VOF methods.

PLIC method, in this paper we propose another approach to reconstruct the interface while retaining simplicity of the implementation.

In Section 2, we describe the simple interface reconstruction algorithm, the WLIC method, the THINC/WLIC method, which is a combination of the WLIC method and the THINC scheme, and the VOF/WLIC method. The numerical experiments of pure advection by these methods and a fluid application (Rayleigh–Taylor instability with surface tension) by the THINC/WLIC method are given in Section 3. The short summary comes in Section 4.

2. Numerical method

2.1. WLIC method

In the WLIC formulation, the interface is reconstructed like the SLIC method or the VOF method by Hirt and Nichols. In order to maintain a simple implementation while taking into account the information of the surface normal more effectively than the SLIC method, we use both the horizontal interface (interface along x-coordinate) and the vertical interface (interface along y-coordinate) as shown in Fig. 5. These interfaces are weighted by using the weights calculated from surface normal $\mathbf{n}$,

$$\chi_{i,j}(x,y) = \omega_{x,i,j}(\mathbf{n}_{i,j})\chi_{x,i,j}(x,y) + \omega_{y,i,j}(\mathbf{n}_{i,j})\chi_{y,i,j}(x,y), \tag{10}$$

where ω_x and ω_y are the weights, and χ_x and χ_y are the characteristic functions of the vertical interface and horizontal interface as shown in Fig. 5, respectively. The weights ω_x and ω_y, and the characteristic functions χ_x and χ_y must satisfy

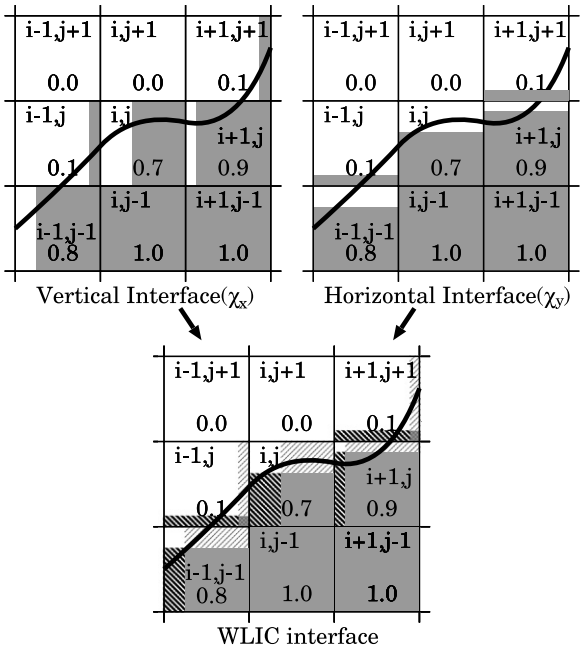

Fig. 5. Schematic figure of the WLIC algorithm.

$$\omega_{x,i,j} + \omega_{y,i,j} = 1, \tag{11}$$

and

$$C_{i,j} = \frac{1}{\Delta x \Delta y} \int\int_{\Omega_{i,j}} \chi_{x,i,j}(x,y)\mathrm{d}x\,\mathrm{d}y = \frac{1}{\Delta x \Delta y} \int\int_{\Omega_{i,j}} \chi_{y,i,j}(x,y)\mathrm{d}x\,\mathrm{d}y. \tag{12}$$

We chose simple weights

$$\omega_{x,i,j} = \frac{|n_{x,i,j}|}{|n_{x,i,j}| + |n_{y,i,j}|}, \tag{13}$$

$$\omega_{y,i,j} = \frac{|n_{y,i,j}|}{|n_{x,i,j}| + |n_{y,i,j}|}. \tag{14}$$

Here, n_x and n_y are x component and y component of surface normal $\mathbf{n}$. The surface normal for the interface is simply calculated by using 3×3 grids:

$$n_{x,i,j} = \frac{1}{4}(n_{x,i+1/2,j+1/2} + n_{x,i-1/2,j+1/2} + n_{x,i+1/2,j-1/2} + n_{x,i-1/2,j-1/2}), \tag{15}$$

$$n_{y,i,j} = \frac{1}{4}(n_{y,i+1/2,j+1/2} + n_{y,i-1/2,j+1/2} + n_{y,i+1/2,j-1/2} + n_{y,i-1/2,j-1/2}), \tag{16}$$

where

$$n_{x,i,j} = \frac{1}{2\Delta x}(C_{i+1,j} - C_{i,j} + C_{i+1,j+1} - C_{i,j+1}), \tag{17}$$

$$n_{y,i,j} = \frac{1}{2\Delta x}(C_{i,j+1} - C_{i,j} + C_{i+1,j+1} - C_{i+1,j}). \tag{18}$$

The WLIC interface is represented as an average of the vertical interface and the horizontal interface as shown in Fig. 5. The flux for the x direction is calculated as

$$F_{x,i+1/2,j} = -\int_{y_{i,j-1/2}}^{y_{i,j+1/2}} \int_{x_{i+1/2,j}}^{x_{x,i+1/2,j}-u_{i+1/2,j}\Delta t} \chi_{is,j}(x,y)\mathrm{d}x\,\mathrm{d}y, \tag{19}$$

$$= -\int_{y_{i,j-1/2}}^{y_{i,j+1/2}} \int_{x_{i+1/2,j}}^{x_{x,i+1/2,j}-u_{i+1/2,j}\Delta t} (\omega_{x,is,j}\chi_{x,is,j}(x,y) + \omega_{y,is,j}\chi_{y,is,j})\mathrm{d}x\,\mathrm{d}y, \tag{20}$$

$$= -\int_{y_{i,j-1/2}}^{y_{i,j+1/2}} \int_{x_{i+1/2,j}}^{x_{x,i+1/2,j}-u_{i+1/2,j}\Delta t} \omega_{x,is,j}\chi_{is,j}\mathrm{d}x\,\mathrm{d}y \tag{21}$$

$$-\int_{y_{i,j-1/2}}^{y_{i,j+1/2}} \int_{x_{i+1/2,j}}^{x_{x,i+1/2,j}-u_{i+1/2,j}\Delta t} \omega_{y,is,j}\chi_{is,j}\mathrm{d}x\,\mathrm{d}y,$$

$$\equiv F_{x,x,i+1/2,j}(\omega_{x,is,j}, \chi_{x,is,j}) + F_{x,y,i+1/2,j}(\omega_{y,is,j}, \chi_{y,is,j}), \tag{22}$$

where $F_{x,y}$ is the flux for the x-direction, which is calculated from ω_y and χ_y. The calculation of flux depends on the numerical methods. The details are explained in the following subsections.

2.2. THINC/WLIC method

The flux $F_{x,x}$ is calculated based on a one-dimensional THINC scheme. As a characteristic function of the THINC scheme, the piecewise modified hyperbolic tangent function[1]:

$$\chi_{x,i} = \frac{1}{2}\left(1 + \alpha_x \tanh\left(\beta\left(\frac{x - x_{i-1/2}}{\Delta x} - \tilde{x}_i\right)\right)\right), \tag{23}$$

[1] Although the maximum value of χ is variable in the original THINC scheme [1], we fixed it to be equal to 1.

is used. Here α_x and β represent the interface direction and smoothing of the characteristic function, respectively. α_x is determined by

$$\alpha_x = \begin{cases} 1 & \text{if } n_{x,i} \geqslant 0, \\ -1 & \text{if } n_{x,i} < 0. \end{cases} \tag{24}$$

Here, we used $n_{x,i} = C_{i+1} - C_{i-1}$. Although we can use $n_{x,i,j}$ of (17), the result by $n_{x,i} = C_{i+1,j} - C_{i-1,j}$ seems better than that by $n_{x,i,j}$ of (17). This $n_{x,i}$ is used only for the calculation of (24). The parameter β determines the steepness of the smoothed Heaviside function. In this paper, we use $\beta = 3.5$ which corresponds one mesh spacing smoothing. $\tilde{x}_i \Delta x$ represents the distance between $x_{i-1/2}$ and the interface, and indicates the position of the interface as shown in Fig. 6a. $\tilde{x}_i$ is calculated from the cell average of χ_i as follows:

$$\frac{1}{\Delta x} \int_{x_{i-1/2}}^{x_{i+1/2}} \chi_i(x, \tilde{x}_i) \mathrm{d}x = C_i^n. \tag{25}$$

The flux $F_{x,x,i+1/2,j}$ is calculated as follows:

$$F_{x,x,i+1/2,j} = -\int_{x_{i+1/2}}^{x_{i+1/2} - u_{i+1/2}\Delta t} \omega_{x,is} \chi_{x,is} \mathrm{d}x, \tag{26}$$

as shown in Fig. 6b. For more detail, see Appendix A. For $F_{x,y,i+1/2}$, the THINC scheme can be described simply as

$$F_{x,y,i+1/2,j} = \omega_{y,is,j} C_{is,j} u_{x,i+1/2,j} \Delta t, \tag{27}$$

because of the definition of $F_{x,y,i+1/2}$ (22). The flux $F_{x,i+1/2,j}$ is calculated by summing (26) and (27).

We can generalize the formulation to two-dimensional case as follows:

$$F_{x,i+1/2,j} = F_{x,x,i+1/2} + F_{x,y,i+1/2}, \tag{28}$$

$$F_{y,i,j+1/2} = F_{y,y,j+1/2} + F_{y,x,j+1/2}, \tag{29}$$

with

$$F_{\xi,\xi,m+1/2} = -\int_{\xi_{m+1/2}}^{\xi_{m+1/2} - u_{m+1/2}\Delta t} \omega_{\xi,ms} \chi_{\xi,ms} \mathrm{d}\xi, \tag{30}$$

$$F_{\xi,\eta,m+1/2} = \omega_{\eta,ms} C_{ms} u_{\xi,m+1/2} \Delta t, \tag{31}$$

$$\chi_{\xi,ms} = \frac{1}{2}\left(1 + \alpha_\xi \tanh\left(\beta\left(\frac{\xi - \xi_{ms-1/2}}{\Delta\xi} - \tilde{\xi}_{ms}\right)\right)\right), \tag{32}$$

$$\alpha_\xi = \begin{cases} 1 & \text{if } n_{\xi,ms} \geqslant 0, \\ -1 & \text{if } n_{\xi,ms} < 0, \end{cases} \tag{33}$$

$$ms = \begin{cases} m & \text{if } u_{\xi,m+1/2} \geqslant 0, \\ m+1 & \text{if } u_{\xi,m+1/2} < 0. \end{cases} \tag{34}$$

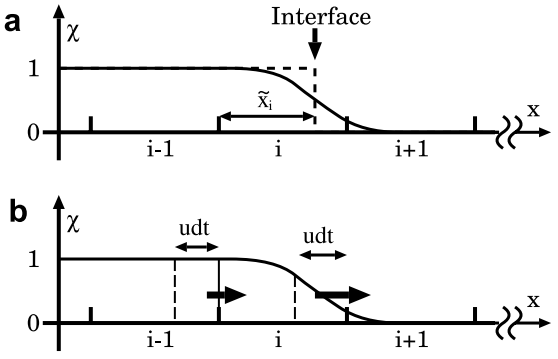

Fig. 6. Schematic figure of the one-dimensional THINC scheme.

The formulation can be easily extended to three-dimensions. Actually, we do not need to alter (30) and (31). A set of fluxes is calculated as follows:

$$F_{x,i+1/2,j,k} = F_{x,i+1/2} = F_{x,x,i+1/2} + F_{x,y,i+1/2} + F_{x,z,i+1/2}, \tag{35}$$

$$F_{y,i,j+1/2,k} = F_{y,j+1/2} = F_{y,x,j+1/2} + F_{y,y,j+1/2} + F_{y,z,j+1/2}, \tag{36}$$

$$F_{z,i,j,k+1/2} = F_{z,k+1/2} = F_{z,x,k+1/2} + F_{z,y,k+1/2} + F_{z,z,k+1/2}. \tag{37}$$

Here, the three-dimensional weights ω_ξ are calculated as follows:

$$\omega_{\xi,m} = \frac{|n_{\xi,m}|}{|n_{x,m}| + |n_{y,m}| + |n_{z,m}|}. \tag{38}$$

Similarly, to two-dimensional case, the three-dimensional formulation can be simplified. We define the following flux:

$$F_{\xi,v,m+1/2} = (1 - \omega_{\xi,ms}) C_{ms} u_{\xi,m+1/2} \Delta t. \tag{39}$$

Here, $F_{\xi,v,m+1/2}$ is the flux calculated from the vertical surfaces for the flux direction, for instance $F_{x,v} = F_{x,y} + F_{x,z}$ (for 3D) and $F_{x,v} = F_{x,y}$ (for 2D). Then we can rewrite (35)–(37) as follows:

$$F_{x,i+1/2} = F_{x,x,i+1/2} + F_{x,v,i+1/2}, \tag{40}$$

$$F_{y,j+1/2} = F_{y,y,j+1/2} + F_{y,v,j+1/2}, \tag{41}$$

$$F_{z,k+1/2} = F_{z,z,k+1/2} + F_{z,v,k+1/2}. \tag{42}$$

Then x and y components of two-dimensional flux (28) and (29) become the same with (40) and (41). Basically, we can use same formula for 2D and 3D except for the weights (surface normal for the interface).

2.3. VOF/WLIC method

The WLIC algorithm can be applied to the VOF formulation as well. The flux of the VOF/WLIC method is calculated like a donor–acceptor scheme [14]. The procedure of the VOF/WLIC method is similar with the THINC/WLIC method. The difference is only the part (30) using the one-dimensional THINC scheme. Other parts have the same formula.

We replace (30) by the donor–acceptor scheme. There are four kinds of flux for $F_{x,x,i+1/2,j}$ as shown in Fig. 7. The formula is

$$F_{\xi,\xi,m+1/2} = \begin{cases} \omega_{\xi,ms} \min(u_{\xi,m+1/2}\Delta t, C_{ms}\Delta\xi) & \text{if } u_{\xi,m+1/2} \geqslant 0 \quad \text{and} \quad n_{\xi,ms} > 0 \\ \omega_{\xi,ms} \max(u_{\xi,m+1/2}\Delta t, -C_{ms}\Delta\xi) & \text{if } u_{\xi,m+1/2} < 0 \quad \text{and} \quad n_{\xi,ms} < 0 \\ \omega_{\xi,ms} \max(0, u_{\xi,m+1/2}\Delta t - (1 - C_{ms})\Delta\xi) & \text{if } u_{\xi,m+1/2} \geqslant 0 \quad \text{and} \quad n_{\xi,ms} < 0 \\ \omega_{\xi,ms} \min(0, u_{\xi,m+1/2}\Delta t + (1 - C_{ms})\Delta\xi) & \text{if } u_{\xi,m+1/2} < 0 \quad \text{and} \quad n_{\xi,ms} > 0. \end{cases} \tag{43}$$

All the other parts are same with the THINC/WLIC method.

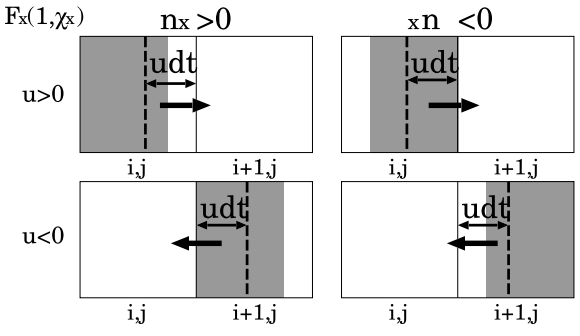

Fig. 7. The schematic figure of the donor–acceptor scheme of the VOF/WLIC method.

3. Numerical results

In order to check the validity of the THINC/WLIC method and to compare the results obtained using the THINC/WLIC with the results obtained using the VOF/WLIC method and the original THINC scheme, these methods are applied to several test problems.

3.1. Advection test of square

These methods were tested by advecting a square step function because some VOF formulations can not treat this test problem well. These results have no significant errors as shown in Figs. 8–10.

3.2. Solid body rotation

Zalesak's test problem [41] in which a notched circle is rotated is widely used as a test of scalar advection method. The velocity field is given by $\mathbf{u} = (y - 0.5, 0.5 - x)$ with $\Delta t = 2\pi/628$. One revolution is completed in

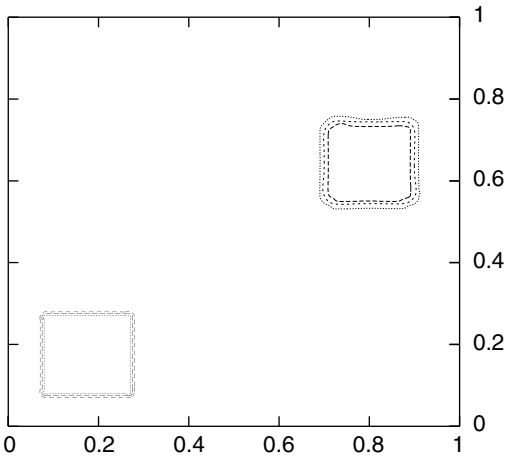

Fig. 8. Advection test of square step function with velocity field (1, 0.75), CFL number 0.25 and 250 steps by the THINC/WLIC method on 100×100 grid.

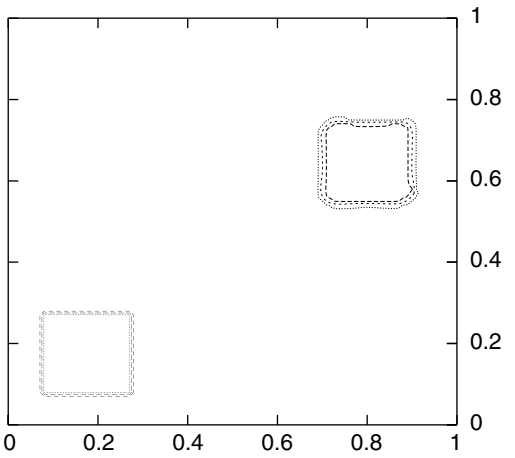

Fig. 9. Advection test of square step function with velocity field (1, 0.75), CFL number 0.25 and 250 steps by the VOF/WLIC method on 100×100 grid.

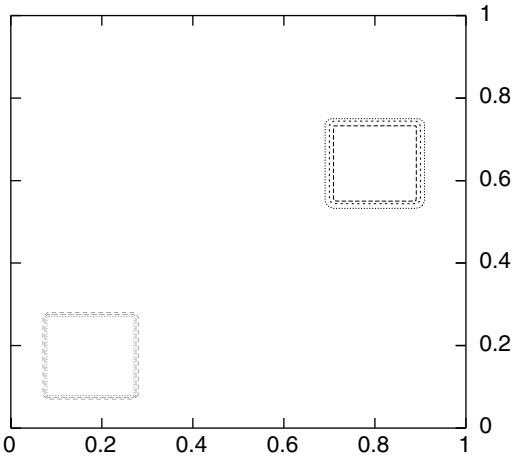

Fig. 10. Advection test of square step function with velocity field (1, 0.75), CFL number 0.25 and 250steps by the original THINC method on 100×100 grid.

628 time steps. Figs. 11–13 represent the results by the THINC/WLIC method, the VOF/WLIC method and the original THINC method, respectively.

Numerical convergence study is performed for Zalesak's problem. Error is defined as

$$\text{Error} = \frac{\Sigma_{i,j}|C^n_{i,j} - C^{\text{ex}}_{i,j}|}{\Sigma_{i,j}C^{\text{ex}}_{i,j}}. \tag{44}$$

Here, $C^{\text{ex}}_{i,j}$ is the exact solution of $C^n_{i,j}$. Table 1 shows the result of the convergence study. Although the THINC/WLIC method and the VOF/WLIC method use the same formulation except for different characteristic functions (smoothed Heaviside function for the THINC method and Heaviside step function for the VOF method), the THINC/WLIC method is superior to the VOF/WLIC method. The THINC/WLIC method and the VOF/WLIC method have first-order accuracy.

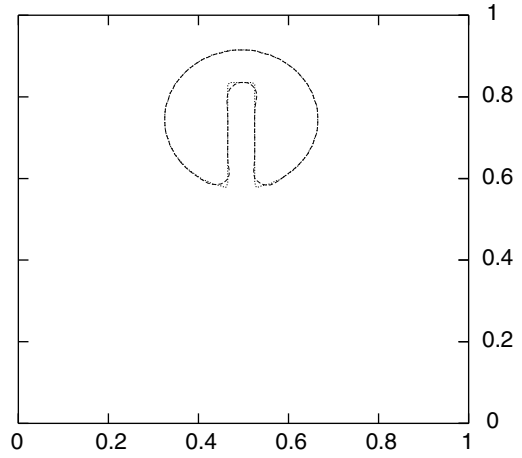

Fig. 11. Zalesak's test problem after one revolution by the THINC/WLIC method on 100×100 grid.

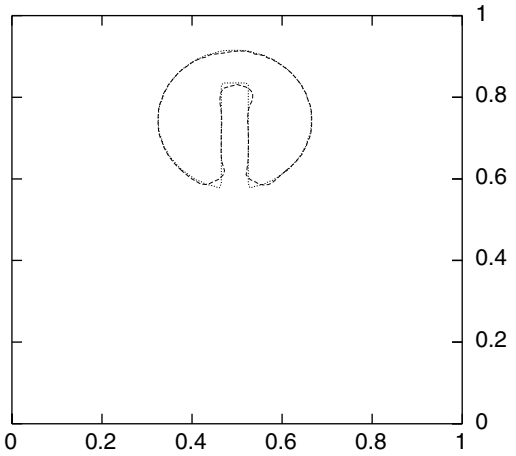

Fig. 12. Zalesak's test problem after one revolution by the VOF/WLIC method on 100×100 grid.

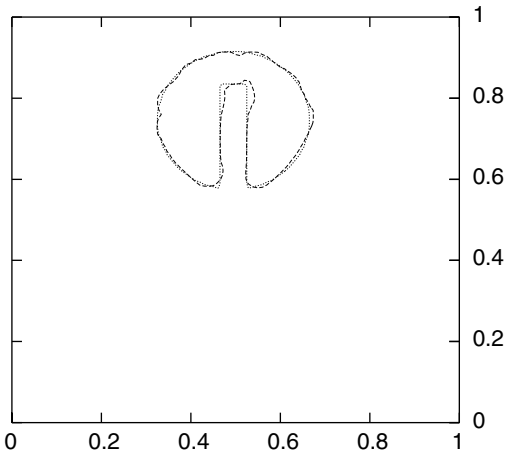

Fig. 13. Zalesak's test problem after one revolution by the original THINC method on 100×100 grid.

Table 1
Errors and convergence rates for Zalesak test problem

Grid spacing	1/50	Rate	1/100	Rate	1/200
THINC/WLIC	1.22×10^{-1}	1.27	5.05×10^{-2}	1.04	2.46×10^{-2}
VOF/WLIC	1.29×10^{-1}	1.26	5.40×10^{-2}	0.75	2.38×10^{-2}
Original THINC	1.32×10^{-1}	0.60	8.73×10^{-2}	0.60	4.79×10^{-2}

3.3. Shearing flow

We apply these methods to a reversed single vertex problem with highly deformed velocity field [17]. The velocity field is defined as

$$\mathbf{u} = (\sin(x)\cos(y), -\cos(x)\sin(y)). \tag{45}$$

The computational domain $[0, \pi] \times [0, \pi]$ is equally divided into a 100×100 mesh. The initial volume fraction distribution is a circle centered at $(\pi/2, (\pi + 1)/5)$ with a radius of $\pi/5$. The initial volume fraction is developed with the velocity field (45) for N steps (the CFL number of 0.25) and then transported back with a reversed

velocity field for another N steps. As expected, the flow field leads to the stretching and spiraling of the initial circle, which is then characterized by a thin film tail that becomes unresolvable by the finite resolution of the fixed mesh when N is large. To compare with the results in [17], we plotted the results for $N = 1000$ and $N = 2000$ in Fig. 14 (THINC/WLIC, $N = 1000$), Fig. 15 (THINC/WLIC, $N = 2000$), Fig. 16 (VOF/WLIC, $N = 1000$), Fig. 17 (VOF/WLIC, $N = 2000$), Fig. 18 (original THINC, $N = 1000$) and Fig. 19 (original THINC, $N = 2000$). Although the VOF/WLIC method produces isolated small fluid bodies (flotsam) which appear in the VOF/SLIC method [16,17,31] as shown in Figs. 16 and 17, the THINC/WLIC method does not generate flotsam as shown in Figs. 14 and 15. Reconstruction using a smoothed Heaviside function of the THINC scheme plays an important role in preventing flotsam. To validate it, we apply the THINC/WLIC method using a steeper smoothed Heaviside function ($\beta = 10$, almost three times steeper than that of $\beta = 3.5$) to the same test problem of $N = 2000$. Then the THINC/WLIC method also generates flotsam as represented in Fig. 20.

Table 2 shows the result of the numerical convergence study. Table 3 represents the errors for different step numbers N. Table 3 shows that the errors by the THINC/WLIC method approach to those by the VOF/PLIC method as deformation becomes larger.

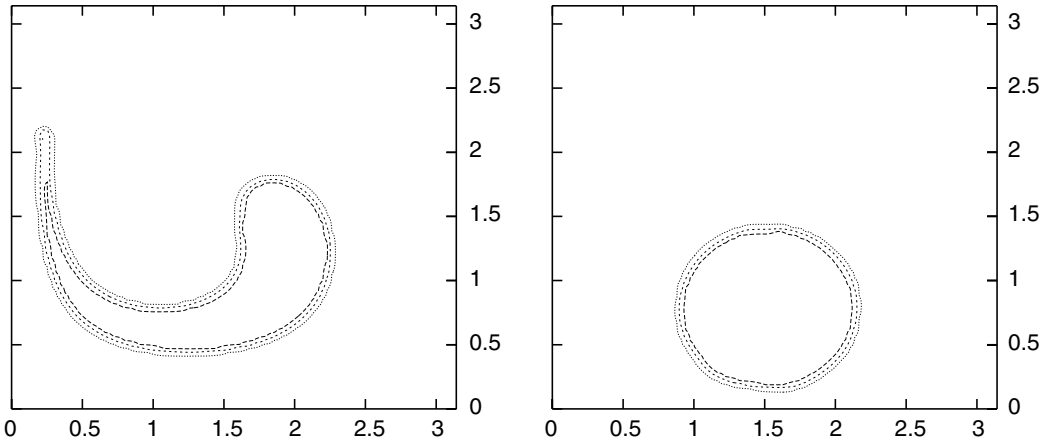

Fig. 14. Single-vortex shearing flow test by THINC/WLIC on 100×100 grid. The left and right figures represent the result after 1000 steps and after 1000 steps forward followed by 1000 steps backward, respectively. The contour levels of 0.05, 0.5 and 0.95 are displayed.

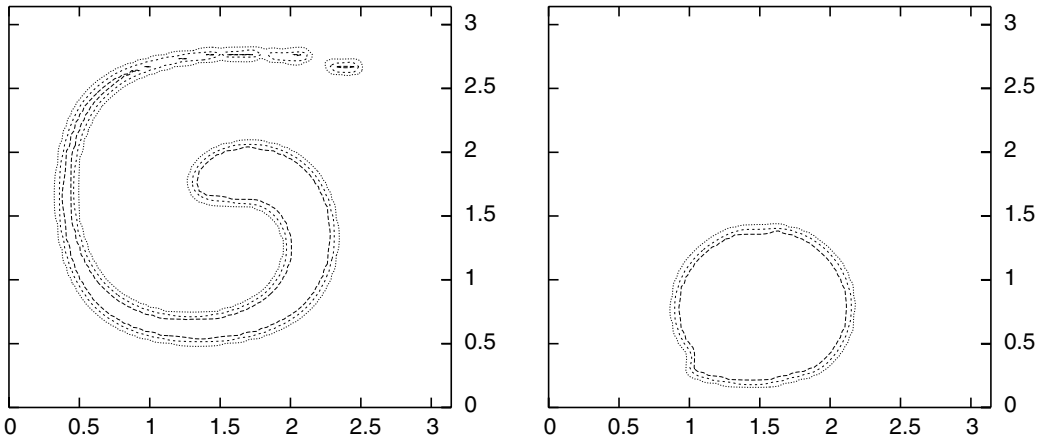

Fig. 15. Single-vortex shearing flow test by THINC/WLIC on 100×100 grid. The left and right figures represent the result after 2000 steps and after 2000 steps forward followed by 2000 steps backward, respectively. The contour levels of 0.05, 0.5 and 0.95 are displayed.

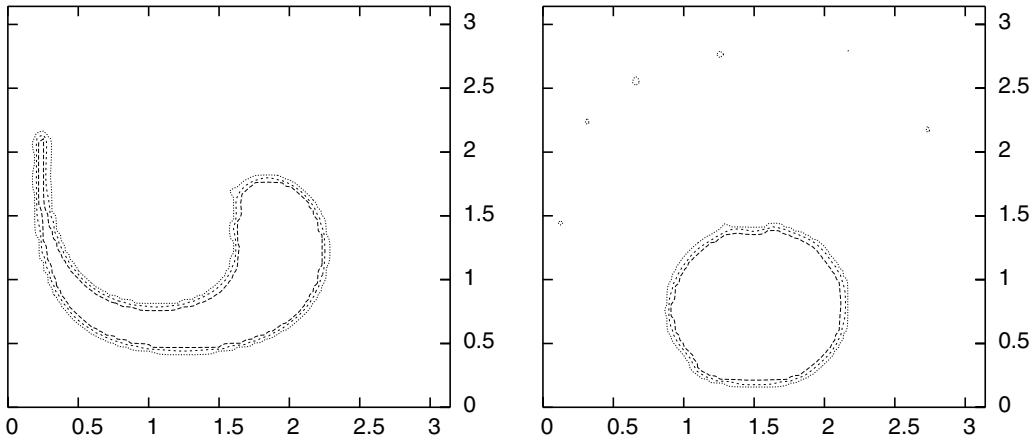

Fig. 16. Single-vortex shearing flow test by VOF/WLIC ($N = 1000$).

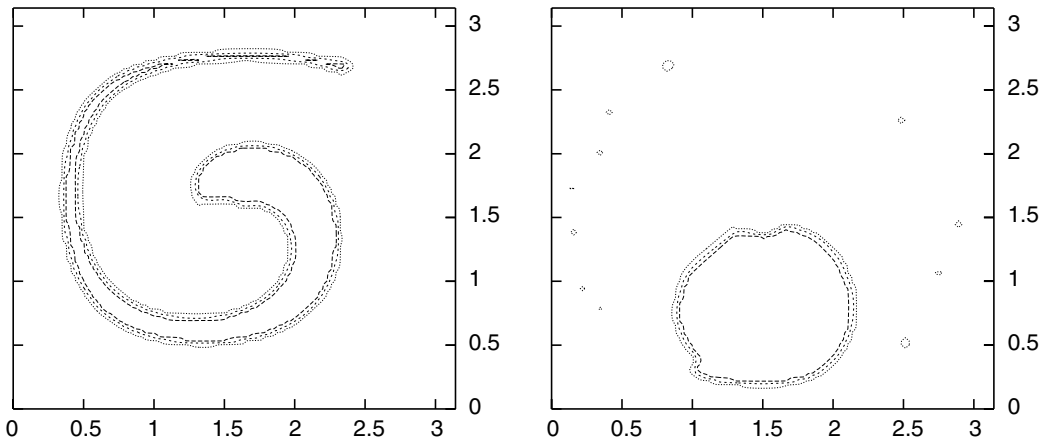

Fig. 17. Single-vortex shearing flow test by VOF/WLIC ($N = 2000$).

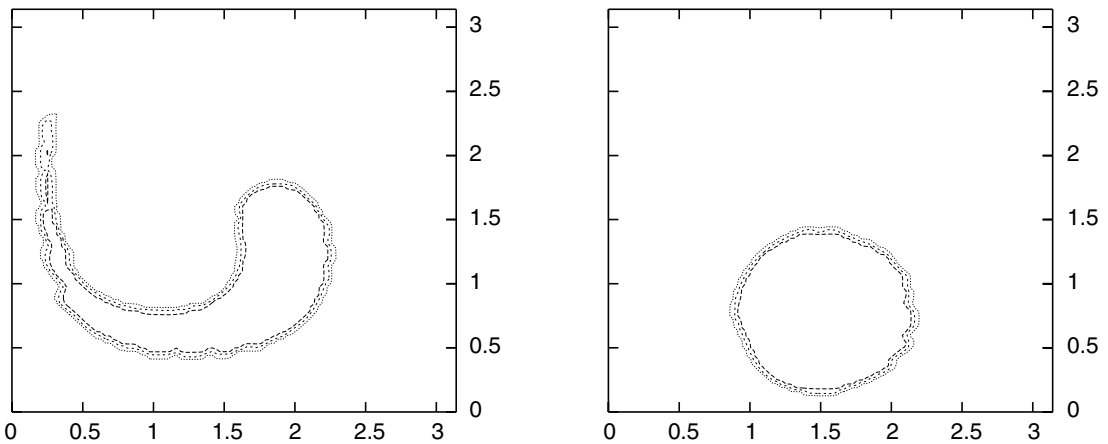

Fig. 18. Single-vortex shearing flow test by the original THINC ($N = 1000$).

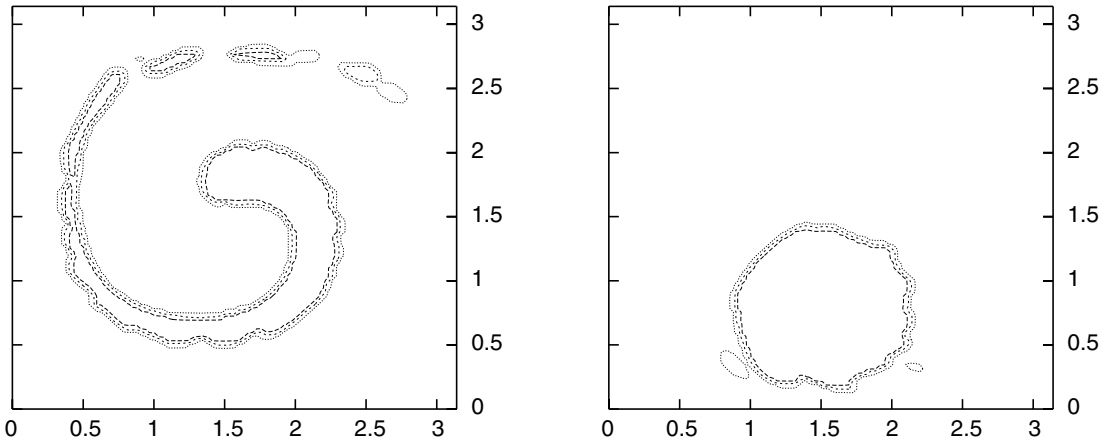

Fig. 19. Single-vortex shearing flow test by the original THINC ($N = 2000$).

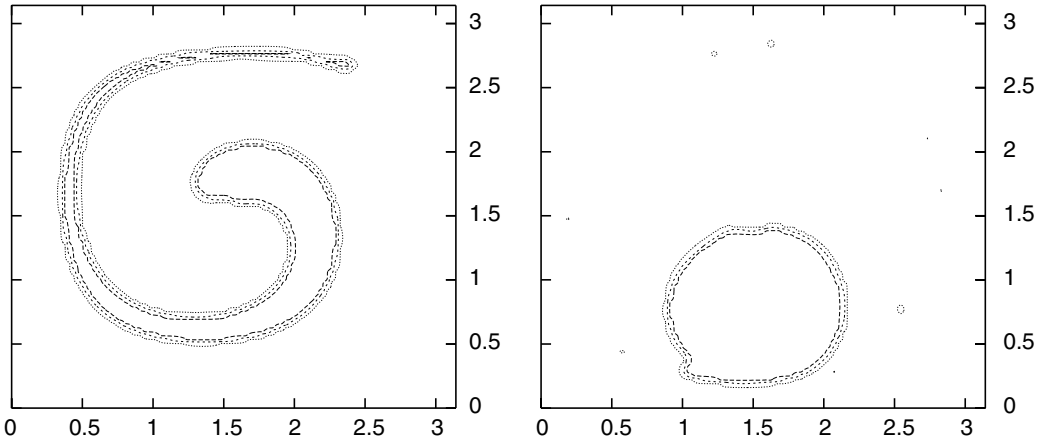

Fig. 20. Single-vortex shearing flow test by the VOF/WLIC method using $\beta = 10$ ($N = 2000$).

Table 2
L_1 errors and convergence rates of shearing flow test with $N = 2000$

Grid spacing	$\pi/50$	Rate	$\pi/100$	Rate	$\pi/200$
THINC/WLIC	1.30×10^{-1}	1.62	4.02×10^{-2}	2.01	1.00×10^{-2}
VOF/WLIC	1.62×10^{-1}	1.36	6.31×10^{-2}	1.65	2.01×10^{-2}
Original THINC	1.57×10^{-1}	1.24	6.64×10^{-2}	0.39	5.06×10^{-2}

Table 3
Errors of shearing flow test with results by other methods for different step number N

Method	Error ($N = 250$)	Error ($N = 500$)	Error ($N = 1000$)	Error ($N = 2000$)
THINC/WLIC	1.11×10^{-2}	1.21×10^{-2}	1.62×10^{-2}	4.02×10^{-2}
VOF/WLIC	1.43×10^{-2}	2.05×10^{-2}	3.28×10^{-2}	6.31×10^{-2}
Original THINC	2.46×10^{-2}	3.13×10^{-2}	3.19×10^{-2}	6.64×10^{-2}
PLIC [17]	2.61×10^{-3}	5.12×10^{-3}	8.60×10^{-3}	3.85×10^{-2}

To compare the orders of accuracy as well as errors of proposed methods with those of a PLIC method [18], THINC/WLIC and VOF/WLIC are applied to another single vertex problem by Rider-Kothe [18,42,43]. The initial volume fraction distribution is a circle centered at (0.5, 0.75) with a radius of 0.15 on the computational domain $[0, 1] \times [0, 1]$. The velocity filed is given by the stream function [18,42,43]:

$$\Psi = \frac{1}{\pi} sin^2(\pi x)\cos^2(\pi y)\cos\left(\frac{\pi t}{T}\right). \tag{46}$$

The initial volume fraction is deformed by the velocity field and it returns to its initial state at $t = T$. A CFL number of one is used. In this test problem, the error is estimated by

$$\text{Error} = \Sigma_{i,j}|C^n_{i,j} - C^{\text{ex}}_{i,j}|\Delta x \Delta y \tag{47}$$

Table 4 shows the result of the numerical convergence study of $T = 8$ with the result by Rider–Kothe [18]. Table 4 exhibits that errors generated by the THINC/WLIC method approach those generated by the VOF/PLIC method for coarser grids.

We compare CPU time of the proposed methods with that of the original VOF by Hirt and Nichols. Compared to the original VOF method, the CPU time of the THINC/WLIC method and the VOF/WLIC method is double and almost same, respectively.

3.4. Fluid simulation

The THINC/WLIC is validated in a fluid simulation with surface tension force. We use following governing equations for incompressible fluid,

$$\int_\Gamma \mathbf{u}\cdot\mathbf{n}\,dS = 0, \tag{48}$$

$$\frac{\partial}{\partial t}\int_\Omega \mathbf{u}\,dV + \int_\Gamma \mathbf{u}(\mathbf{u}\cdot\mathbf{n})dS = -\frac{1}{\rho}\int_\Gamma p\mathbf{n}\,dS + \frac{1}{\rho}\int_\Gamma \boldsymbol{\tau}\cdot\mathbf{n}\,dS + \mathbf{F}_{\text{sf}} + \mathbf{F}_{\text{bf}} \tag{49}$$

where $\mathbf{u}$ is the velocity, $\mathbf{n}$ the outgoing normal vector for the control volume Ω with its surface denoted by Γ, ρ the density, p the pressure, $\boldsymbol{\tau}$ the viscous stress tensor, $\mathbf{F}_{\text{sf}}$ the surface tension force and $\mathbf{F}_{\text{bf}}$ the body force. These equations are solved by the CIP-CSL(constrained interpolation profile conservative semi-Lagrangian) method [44–46] of a conservation equation solver and VSIAM3 (volume/surface integrated average based multi-moment method) [47,48] of a fluid solver. The CSF (continuum surface force) model [50] is used for the surface tension computation. For the curvature calculation, the level set function (a signed distance function) is created from 0.5 contour of the VOF function by a CLSVOF (coupled level set and volume-of-fluid) framework [9,10]. The detail of the fluid algorithm will be reported in [54].

The Rayleigh–Taylor instability with surface tension force is computed [49–51]. When a heavy fluid is supported against gravity by a light fluid, a Rayleigh–Taylor instability develops in which perturbations of the interface grow exponentially in time as $\exp(nt)$ for small amplitudes. The growth rate n is given by [52,53]

$$n^2 = Kg\left[A - \frac{K^2\sigma}{g(\rho_{\text{l}} - \rho_{\text{h}})}\right], \tag{50}$$

where K is the wave number of the perturbation, g the gravity acceleration, $A = (\rho_{\text{h}} - \rho_{\text{l}})/(\rho_{\text{l}} + \rho_{\text{h}})$, and ρ_{l} and ρ_{h} are the densities of the light fluid and heavy fluid, respectively. Following Daly [49], a stability parameter Φ can be defined:

$$\Phi = \frac{\sigma}{\sigma_{\text{c}}} = \frac{\sigma K^3}{(\rho_{\text{h}} - \rho_{\text{l}})g} \tag{51}$$

where σ_{c} is a critical value of the surface tension coefficient for $n = 0$. For $\sigma_{\text{c}} < 1$, the interface with a perturbation leads to instability.

Table 4
Errors and convergence rates of shearing flow test of Rider–Kothe ($T = 8$)

Grid spacing	1/32	Rate	1/64	Rate	1/128	Rate	1/256
THINC/WLIC	4.88×10^{-2}	1.75	1.45×10^{-2}	2.40	2.75×10^{-3}	1.94	7.24×10^{-4}
VOF/WLIC	5.81×10^{-2}	1.79	1.68×10^{-2}	2.53	2.90×10^{-3}	1.39	1.11×10^{-3}
PLIC [18]	4.78×10^{-2}	2.78	6.96×10^{-3}	2.27	1.44×10^{-3}	–	–

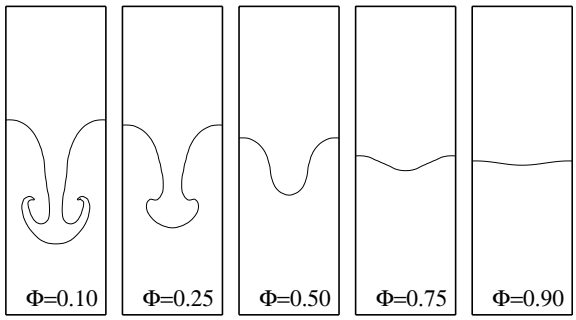

Fig. 21. Snapshots of the Rayleigh–Taylor instability at $t = 13$ for several values of Φ. A 40×120 grid was used.

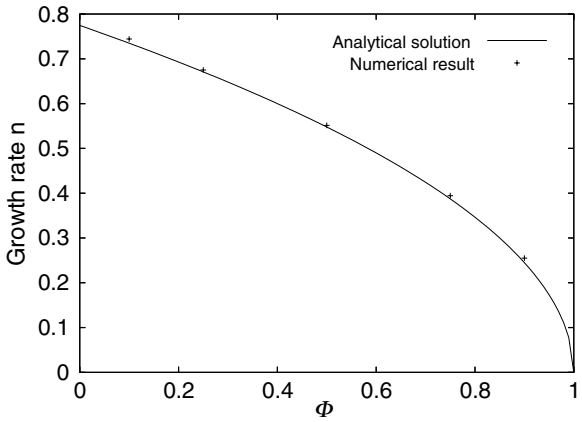

Fig. 22. Theoretical Rayleigh–Taylor instability growth rate (line) and computed growth rates (dot) are plotted as a function of the stability parameter Φ.

Fig. 21 shows snapshots of the Rayleigh–Taylor instability at $t = 13$ for several values of Φ. As a set of parameters, $\rho_l = 0.25$, $\rho_h = 1.0$, $K = 1$, $g = 1$ and $\mu = 0$ are used, where μ is the viscosity coefficient. The domain width and height are 2π and 6π, respectively. The instability is initiated with a perturbation $\delta v \cos(Kx)$ ($\delta v = 5 \times 10^{-3}$ is used in this paper) given to the vertical velocity component at the interface. A 40×120 grid was used. The boundary condition on top and bottom boundaries is Neumann. For side boundaries, the periodic boundary condition is used. The growth rates of numerical simulations are compared with the analytical solution in Fig. 22.

4. Summary

We proposed a simple and practical VOF type method based on the THINC scheme. A simple interface reconstruction algorithm (WLIC) was proposed and combined with the THINC scheme. Although the THINC/WLIC method is a kind of stair-stepped method like the VOF method by Hirt and Nichols [14], the numerical results obtained using the THINC/WLIC method might appear to be similar to those obtained using the VOF/PLIC method. The results by the THINC/WLIC method approach those by the VOF/PLIC method for larger deformations and coarser grids. However the THINC/WLIC method is not superior to the VOF/PLIC method. The implementation of the THINC/WLIC method is simpler than that of the VOF/PLIC method. The THINC/WLIC method can be naturally extended to three-dimensions. An appropriate interface smoothness plays an important role in preventing flotsam. The numerical results of the Rayleigh–Taylor instability with surface tension force show good agreement with the theoretical solution.

Acknowledgements

We thank Feng Xiao, Stanley Osher, Hao Liu, Jeremy Brandman, Igor Yanovsky and Jason Chung for useful discussions, comments and supports. Numerical computations in this work were partially carried out on SX8 at the Yukawa Institute for Theoretical Physics, Kyoto University. We also acknowledge the supports of Institute for Pure and Applied Mathematics (IPAM).

Appendix A. One-dimensional THINC

$\tilde{x}_i$ and $F_{x,x,i+1/2}$ are calculated as follows:

$$C_i = \frac{1}{\Delta x}\int_{x_{i-1/2}}^{x_{i+1/2}} \frac{1}{2}\left(1+\alpha\tanh\left(\beta\left(\frac{x-x_{i-1/2}}{\Delta x}-\tilde{x}_i\right)\right)\right)\mathrm{d}x, \tag{A.1}$$

$$C_i = \frac{1}{2\Delta x}\left[x+\frac{\alpha\Delta x}{\beta}\ln\left(\cosh\left(\beta\left(\frac{x-x_{i-1/2}}{\Delta x}\right)-\tilde{x}_i\right)\right)\right]_{x_{i-1/2}}^{x_{i+1/2}}, \tag{A.2}$$

$$C_i = \frac{1}{2}\left(1+\frac{\alpha}{\beta}\ln\left(\frac{\cosh(\beta(1-\tilde{x}_i))}{\cosh(\beta\tilde{x}_i)}\right)\right), \tag{A.3}$$

$$C_i = \frac{1}{2}\left(1+\frac{\alpha}{\beta}\ln a_1\right). \tag{A.4}$$

Here,

$$a_1 \equiv \frac{\cosh(\beta(1-\tilde{x}_i))}{\cosh(\beta\tilde{x}_i)} = \exp\left(\frac{\beta}{\alpha}(2C_i-1)\right), \tag{A.5}$$

$$a_1 = \frac{\exp(\beta(1-\tilde{x}_i))+\exp(-\beta(1-\tilde{x}_i))}{\exp(\beta\tilde{x}_i)+\exp(-\beta\tilde{x}_i)} = \frac{a_3^2+a_2^2}{a_3(a_2^2+1)}. \tag{A.6}$$

Here,

$$a_2 \equiv \exp(\beta\tilde{x}_i), \tag{A.7}$$

$$a_3 \equiv \exp(\beta), \tag{A.8}$$

$$a_2^2 = \frac{a_3^2-a_1a_3}{a_1a_3-1}, \tag{A.9}$$

then

$$\tilde{x}_i = \frac{1}{2\beta}\ln\left(\frac{a_3^2-a_1a_3}{a_1a_3-1}\right). \tag{A.10}$$

The flux is calculated as follows:

$$F_{x,x,i+1/2} = -\int_{x_{i+1/2}}^{x_{i+1/2}-u_{i+1/2}\Delta t}\frac{\omega_{x,is}}{2}\left(1+\alpha\tanh\left(\beta\left(\frac{x-x_{is-1/2}}{\Delta x}-\tilde{x}_{is}\right)\right)\right)\mathrm{d}x, \tag{A.11}$$

$$= -\frac{\omega_{x,is}}{2}\left[x+\frac{\alpha\Delta x}{\beta}\ln\left(\cosh\left(\beta\left(\frac{x-x_{is-1/2}}{\Delta x}\right)-\tilde{x}_{is}\right)\right)\right]_{x_{i+1/2}}^{x_{i+1/2}-u_{i+1/2}\Delta t}. \tag{A.12}$$

References

[1] F. Xiao, Y. Honma, T. kono, A simple algebraic interface capturing scheme using hyperbolic tangent function, Int. J. Numer. Meth. Fluid. 48 (2005) 1023.
[2] S.O. Unverdi, G. Tryggvason, A front tracking method for viscous, incompressible multi-fluid flow, J. Comput. Phys. 100 (1992) 25.
[3] J. Glimm et al., Front tracking in two and three dimensions, J. Comput. Mech. 7 (1998) 1.

[4] S. Osher, J.A. Sethian, Front propagating with curvature-dependent speed: algorithms based on Hamilton–Jacobi formulation, J. Comput. Phys. 79 (1988) 12.
[5] M. Sussman, P. Smereka, S. Osher, A level set approach for capturing solution to incompressible two-phase flow, J. Comput. Phys. 114 (1994) 146.
[6] M. Sussman, P. Smereka, Axisymmetric free boundary problems, J. Fluid Mech. 341 (1997) 269.
[7] M. Sussman, E. Fatemi, An efficient, interface preserving level set re-distancing algorithm and its application to interfacial incompressible fluid flow, SIAM J. Sci. Comput. 20 (1999) 1165.
[8] J.A. Sethian, Level Set Methods and Fast Marching Methods, Cambridge University Press, 1999.
[9] M. Sussman, E.G. Puckett, A coupled level set and volume-of-fluid method for computing 3D and axisymmetric incompressible two-phase flows, J. Comput. Phys. 162 (2000) 301–337.
[10] K. Yokoi, Numerical method for complex moving boundary problems in a Cartesian fixed grid, Phys. Rev. E 65 (2002) 055701(R).
[11] D. Enright, R. Fedkiw, J. Ferziger, I. Mitchell, A hybrid particle level set method for improved interface capturing, J. Comput. Phys. 183 (2002) 83–116.
[12] S. Osher, R. Fedkiw, Level set methods and dynamics implicit surface, Applied Mathematical Sciences, vol. 153, Springer, 2003.
[13] W.F. Noh, P. Woodward, SLIC (simple line interface method), Lecture Notes in Physics 24 (1976) 330.
[14] C.W. Hirt, B.D. Nichols, Volume of fluid (VOF) methods for the dynamic of free boundaries, J. Comput. Phys. 39 (1981) 201.
[15] D.L. Youngs, Time-dependent multi-material flow with large fluid distortion, in: K.W. Morton, M.J. Baines (Eds.), Numerical Methods for Fluid Dynamics, vol. 24, Academic Press, New York, 1982, pp. 273–285.
[16] B. Lafaurie, C. Nardone, R. Scardovelli, S. Zaleski, G. Zanetti, Modeling merging and fragmentation in multiphase flows with SURFER, J. Comput. Phys. 113 (1994) 134–147.
[17] M. Rudman, Volume-tracking method for interfacial flow calculations', Int. J. Numer. Meth. Fluids 24 (1997) 679–691.
[18] W.J. Rider, D.B. Kothe, Reconstructing volume tracking, J. Comput. Phys. 141 (1998) 112.
[19] R. Scardovelli, S. Zaleski, Direct numerical simulation of free-surface and interfacial flow, Annu. Rev. Fluid Mech. 31 (1999) 567–603.
[20] J. Li, Y. Renardy, M. Renardy, Numerical simulation of breakup of a viscous drop in simple shear flow with a volume-of-fluid method, Phys. Fluids 12 (2000) 269–282.
[21] D.J.E. Harvie, D.F. Fletcher, A new volume of fluid advection algorithm: the stream scheme, J. Comput. Phys. 162 (2000) 1–32.
[22] D.J.E. Harvie, D.F. Fletcher, A new volume of fluid advection algorithm: the defined donating region scheme, Int. J. Numer. Meth. Fluids 35 (2001) 151–172.
[23] Y. Renardy, V. Cristini, Effect of inertia on drop breakup under shear, Phys. Fluids 13 (2001) 7.
[24] Y. Renardy, M. Renardy, V. Cristini, A new volume-of-fluid formulation for surfactants and simulations of drop deformation under shear at a low viscosity ratio, Eur. J. Mech. B/Fluids 21 (2002) 49.
[25] Y. Renardy, V. Cristini, J. Li, Drop fragment distribution under shear with inertia, Int. J. Multiphase Flow 28 (2002) 1125–1147.
[26] D. Khismatullin, Y. Renardy, V. Cristini, Inertia-induced breakup of highly viscous drops subjected to simple shear, Phys. Fluids 15 (2003) 1351.
[27] E. Aulisa, S. Manservisi, R. Scardovelli, A mixed markers and volume-of-fluid method for the reconstruction and advection of interfaces in two-phase and free-boundary flows, J. Comput. Phys. 188 (2003) 611–639.
[28] J. Lopez, J. Hernandez, P. Gomez, F. Faura, A volume of fluid method based on multidimensional advection and spline interface reconstruction, J. Comput. Phys. 195 (2004) 718–742.
[29] E. Aulisa, S. Manservisi, R. Scardovelli, S. Zaleski, A geometrical area-preserving volume-of-fluid advection method, J. Comput. Phys. 192 (2004) 355–364.
[30] E. Aulisa, S. Manservisi, R. Scardovelli, A surface marker algorithm coupled to an area-preserving marker redistribution method for three-dimensional interface tracking, J. Comput. Phys. 197 (2004) 555–584.
[31] J.E. Pilliod, E.G. Puckett, Second-order accurate volume-of-fluid algorithms for tracking material interfaces, J. Comput. Phys. 199 (2004) 465–502.
[32] V. Cristini, Y.C. Tan, Theory and numerical simulation of droplet dynamics in complex flows, Lab Chip 4 (2004) 257.
[33] J. Lopez, J. Hernandez, P. Gomez, F. Faura, An improved PLIC-VOF method for tracking thin fluid structures in incompressible two-phase flows, J. Comput. Phys. 208 (2005) 51–74.
[34] X. Yang, A.J. James, J. Lowengrub, X. Zheng, V. Cristini, An adaptive coupled level-set/volume-of-fluid interface capturing method for unstructured triangular grids, J. Comput. Phys. 217 (2) (2006) 364–394.
[35] V. Cristini, Y. Renardy, Scalings for droplet sizes in shear-driven breakup: non-microfluidic ways to monodisperse emulsions, Fluid Dyn. Mater. Process. 2 (2) (2006).
[36] E. Aulisa, S. Manservisi, R. Scardovelli, S. Zaleski, Interface reconstruction with least-squares fit and split advection in three-dimensional Cartesian geometry, J. Comput. Phys., in press. doi:10.1016/j.jcp.2007.03.015.
[37] R. Fedkiw, T. Aslam, B. Merriman, S. Osher, A non-oscillatory Eulerian approach to interfaces in multimaterial flows (the ghost fluid method), J. Comput. Phys. 152 (1999) 457–492.
[38] K. Yokoi, Numerical method for moving solid object in flows, Phys. Rev. E 67 (2003) 045701(R).
[39] S. Marella, S. Krishnan, H. Liu, H.S. Udaykumar, Sharp interface Cartesian grid method I: an easily implemented technique for 3D moving boundary computations, J. Comput. Phys. 210 (2005) 1.
[40] M. Sussman, K.M. Smith, M.Y. Hussaini, M. Ohta, R. Zhi-Wei, A sharp interface method for incompressible two-phase flows, J. Comput. Phys. 221 (2007) 469–505.
[41] S.T. Zalesak, Fully multi-dimensional flux corrected transport algorithm for fluid flow, J. Comput. Phys. 31 (1979) 335.

[42] J.B. Bell, P. Colella, H.M. Glaz, A second-order projection method of the incompressible Navier–Stokes equations, J. Comput. Phys. 85 (1989) 257.
[43] R. LeVeque, High-resolution conservative algorithms for advection in incompressible flow, SIAM J. Numer. Anal. 33 (1996) 627–665.
[44] R. Tanaka, T. Nakamura, T. Yabe, Constructing exactly conservative scheme in a non-conservative form, Comput. Phys. Commun. 126 (2000) 232.
[45] T. Yabe, F. Xiao, T. Utsumi, Constrained interpolation profile method for multiphase analysis, J. Comput. Phys. 169 (2001) 556.
[46] F. Xiao, T. Yabe, X. Peng, H. Kobayashi, Conservative and oscillation-less atmospheric transport schemes based on rational functions, J. Geophys. Res. 107 (2002) 4609.
[47] F. Xiao, A. Ikebata, T. Hasegawa, Numerical simulations of free-interface fluids by a multi integrated moment method, Comp. Struct. 83 (2005) 409–423.
[48] F. Xiao, R. Akoh, S. Ii, Unified formulation for compressible and incompressible flows by using multi integrated moments II: multi-dimensional version for compressible and incompressible flows, J. Comput. Phys. 213 (2006) 31–56.
[49] B.J. Daly, Numerical study of the effect of surface tension on interface instability, Phys. Fluids 12 (1969) 1340.
[50] J.U. Brackbill, D.B. Kothe, C. Zemach, A continuum method for modeling surface tension, J. Comput. Phys. 100 (1992) 335.
[51] D. Gerlach, G. Tomar, G. Biswas, F. Durst, Comparison of volume-of-fluid methods for surface tension-dominant two-phase flows, Int. J. Heat Mass Transfer 49 (2006) 740.
[52] R. Bellman, R.H. Pennington, Effect of surface tension and viscosity on Taylor instability, Quart. Appl. Meth. 12 (12) (1954) 151.
[53] P.G. Drazin, W.H. Reid, Hydrodynamic Stability, Cambridge University Press, Cambridge, UK, 1967.
[54] K. Yokoi, A numerical method for free-surface flows and its application to droplet impact on a thin liquid layer, J. Sci. Comp., submitted for publication.